

# NUMERICAL STUDY ON FREQUENCY DOWNSHIFT OF GRAVITY WAVE SPECTRA IN DEEP AND INTERMEDIATE WATER DEPTHS DUE TO NONLINEAR ENERGY TRANSFER

Noriaki Hashimoto<sup>1</sup> Fitri Suciaty<sup>1</sup>, Masaru Yamashiro<sup>1</sup>,  
Masaki Yokota<sup>1</sup>, and Mitsuyoshi Kodama<sup>1</sup>

Frequency downshift of gravity wave spectra in deep and finite water depths due to the nonlinear energy transfer are discussed. In deep water depths, numerical computations of the nonlinear energy transfer are performed with DIA (Hasselmann et al., 1985), RIAM (Komatsu et al., 1993) and SRIAM (Komatsu et al., 1996). Then, differences in temporal changes of directional spectra computed with a modified WAM implemented with RIAM and SRIAM are compared with those computed with the original WAM implemented with DIA. In finite water depth, numerical computations are performed with a modified WAM implemented with FD-RIAM (Hashimoto, et al., 2002), an exact method, which was upgraded from an earlier version (Hashimoto et al., 1998) based on Komatsu et al., (2001). Differences in frequency downshift of gravity wave spectra in deep and finite water depths are discussed based on the numerical results for various directional spectra in various water depths.

*Keywords: nonlinear energy transfer; frequency downshift; wave modeling*

## INTRODUCTION

Long period waves ranging from 15 to over 25 seconds occasionally cause damage to coastal structures. Nevertheless, the mechanism of the generation and development of the waves has not been clarified. The reproducibility of the long period waves by existing wave models has not been discussed thoroughly so far. We therefore numerically investigate characteristics of frequency downshift of directional spectra by considering the nonlinear energy transfer in deep and intermediate water depths as a possible mechanism.

There are many researches which have been performed in the past decades to compute nonlinear energy transfer. In 1960, Phillips found the dynamics of unsteady gravity waves of finite amplitude, and Hasselmann derived the Boltzmann integral in 1962. Following Hasselmann (1962,1963), a set of four waves exchange the energy when the following resonance conditions are satisfied:

$$\mathbf{k}_1 + \mathbf{k}_2 = \mathbf{k}_3 + \mathbf{k}_4 \quad (1)$$

$$\omega_1 + \omega_2 = \omega_3 + \omega_4 \quad (2)$$

where  $\omega_i$  is the angular frequency and  $\mathbf{k}_i$  the wave number vector ( $i=1,\dots,4$ ). The angular frequency  $\omega_i$  and the wave number  $k_i$  are related through the dispersion relationship ( $\omega_i^2 = gk_i \tanh k_i h$ ). Then, the nonlinear energy transfer can be computed with the following Boltzmann integral (Hasselmann, 1962):

$$\frac{\partial n(\mathbf{k}_4)}{\partial t} = \int \dots \int d\mathbf{k}_1 d\mathbf{k}_2 d\mathbf{k}_3 G(\mathbf{k}_1, \mathbf{k}_2, \mathbf{k}_3, \mathbf{k}_4) \times \delta(\mathbf{k}_1 + \mathbf{k}_2 - \mathbf{k}_3 - \mathbf{k}_4) \delta(\omega_1 + \omega_2 - \omega_3 - \omega_4) \quad (3)$$

$$\times \{n_1 n_2 (n_3 + n_4) - n_3 n_4 (n_1 + n_2)\}$$

where  $n_i = n(\mathbf{k}_i) = \Phi(\mathbf{k}_i)/\omega_i$  is the wave action density,  $\Phi(\mathbf{k}_i)$  is the wave number spectrum, and  $G(\mathbf{k}_1, \mathbf{k}_2, \mathbf{k}_3, \mathbf{k}_4)$  is the coupling coefficient.

The computation of the Boltzmann integral consists of a six-dimensional integrals, a complicated coupling coefficient, and two delta functions corresponding to the resonance conditions. Several computation techniques have been proposed for the solution of the Boltzmann integral. Hasselmann (1963), Sell and Hasselmann (1972), Webb (1978), and Masuda (1980) reduced the six-fold integral into a three-fold integral which contributed to the improvement of the computational speed. The EXACT-NL which proposed by Hasselmann and Hasselmann (1985), the WRT code of Webb (1978) and Tracy and Resio (1982) were some efforts which also accelerated the calculation in the past (Young, 1999).

The biggest advance in the spectral wave model for nonlinear energy transfer was the development of the Discrete Interaction Approximation (DIA) by Hasselmann et al. (1985), having been adopted by most of the third generation wave models, such as WAM, SWAN, and WW3. The DIA has been the

---

<sup>1</sup> Kyushu University, 744 Motoooka Nishi-ku Fukuoka 819-0395, Japan

state of the art tool for calculating the nonlinear energy transfer in practical wave forecasting methods for more than two decades (Roland, 2009). However, the DIA does not have sufficient accuracy for sharp-pointed shape spectra such as the JONSWAP type spectrum, although it gives good performance for broader shape spectra such as the Pierson-Moskowitz spectrum (Hashimoto and Kawaguchi, 2001).

This study evaluates the frequency downshift of directional spectra computed by a third generation wave model, WAM, with several computation methods of the nonlinear energy transfer such as DIA, RIAM (Komatsu et al., 1993) and SRIAM (Komatsu et al., 1996) in deep water waves. Numerical simulations are carried out with a modified WAM (implemented with RIAM and SRIAM) to know the characteristic of the nonlinear energy transfer in relation to the various shapes of directional spectra in deep water depth. Differences between a modified WAM and the original WAM are also discussed.

Similarly, we evaluate the frequency downshift of directional spectra computed with a modified WAM implemented with FD-RIAM (Hashimoto, et al., 2002) in deep water waves, where FD-RIAM is an accurate method for computing the nonlinear energy transfer in finite water depth, which was upgraded from an earlier version (Hashimoto et al., 1998) based on Komatsu et al., (2001). Numerical simulations are carried to investigate characteristics of duration-limited evolutions as well as frequency downshift in various shapes of directional spectra in various water depths. Then, we evaluate characteristics of the enhancement factor  $R$  used in most of the third generation wave models for the computation of the nonlinear energy transfer in finite water depth. Moreover, we also discuss the downshift factor for various directional spectra in various water depths.

## NUMERICAL SIMULATIONS

### Computation methods of the nonlinear energy transfer

Masuda (1980) developed an accurate computation method by deriving approximate solution around the singular points of the Boltzmann integral. Komatsu et al.(1993) developed RIAM method by modifying Masuda's method with the use of symmetry characteristics of the resonant four waves. The computation of RIAM method is 300 times faster than Masuda's method, yet restricted to deep water wave applications. Komatsu and Masuda (1996) simplified RIAM into SRIAM which makes the computation 100 times faster than RIAM. The SRIAM method, however, requires a computation time 20 times longer than DIA. SRIAM is one of the important progress which has been made in optimizing the interactions, yet more expensive than DIA, making it economically unacceptable for application in a practical model at the moment (Tolman, 2003).

In this study, the computations of frequency downshift due to the nonlinear energy transfer are performed with DIA, RIAM, and SRIAM for deep water waves, and FD-RIAM for finite water waves. These methods are briefly explained below, following Hashimoto et al. (2002).

**RIAM method (accurate method)**The RIAM method was developed from the initial work of Masuda (1980) who derived a reduction of the six-fold Boltzmann integral to a three-fold integral by taking the independent parameters  $(\theta_1, \omega_3, \theta_3)$  as expressed by the following equation;

$$\frac{\partial \phi_4}{\partial t} = (2\omega_4^{23}) \int_0^\pi d\tilde{\theta}_3 \int_0^\pi d\tilde{\Omega} \int_0^\pi d\tilde{\theta}_1 \sum_{\pm} \sum_{\pm} \sum_{\pm} (8\tilde{\omega}_1^3 \tilde{\omega}_3^4 \tilde{G} S^{-1}) \{n_1 n_2 (n_3 + n_4) - n_3 n_4 (n_1 + n_2)\} \quad (4)$$

where,  $|\mathbf{k}_1| \leq |\mathbf{k}_2|$  (or  $\omega_1 \leq \omega_2$ ) is assumed without loss of generality from the symmetry of Eq. (3).

The variables are non-dimensionalised by

$$\tilde{\theta}_1 = \theta_1 - \theta_a, \quad \tilde{\theta}_2 = \theta_2 - \theta_a, \quad \tilde{\theta}_3 = \theta_3 - \theta_a, \quad \tilde{\omega}_1 = \omega_1 / \omega_4, \quad \tilde{\omega}_2 = \omega_2 / \omega_4, \quad \tilde{\omega}_3 = \omega_3 / \omega_4,$$

and  $\tilde{\Omega} = \ln \tilde{\omega}_3$ .

The denominator  $S$  arising from  $\delta(\omega_1 + \omega_2 - \omega_3 - \omega_4)$  is given by

$$S = \left| 1 + (\omega_1 / \omega_2) \{ (\omega_1 / \omega_2)^2 - (|\mathbf{k}_a| / \omega_2^2) \cos(\theta_1 - \theta_a) \} \right| \quad (5)$$

As Masuda noted, a numerical instability in the integration of Eq. (4) is caused mainly by inappropriate treatment of singular points. Masuda hence solved this instability problem by analytically deriving an approximate solution of Eq. (4) around the singular points.

In order to improve the performance of wave models with the above technique of Masuda and to gain better physical understanding of the spectral evolution, Komatsu and Masuda (1996) developed a new scheme called the RIAM method (RIAM = Research Institute for Applied Mechanics, Kyushu University, Japan) for calculating the nonlinear energy transfer on the basis of the rigorous method of

Masuda (1980). This new scheme was developed by taking advantage of the symmetry of the integrand as in Hasselmann and Hasselmann (1981) or Resio and Perrie (1991), and by truncating less significant configurations of resonance to achieve a shorter computational time without loss of accuracy.

As Komatsu and Masuda (1996) mentioned, there are two kinds of symmetries in the resonant interaction. The first is based on the well-known nature of non-linear resonant interactions among gravity waves expressed by Eq. (1). As explained in Hasselmann and Hasselmann (1981),  $\delta n(\mathbf{k}_i)d\mathbf{k}_i/\delta t$  ( $i=1, 2, 3, 4$ ) have the following relationship:

$$\frac{\delta n(\mathbf{k}_1)}{\delta t}d\mathbf{k}_1 = \frac{\delta n(\mathbf{k}_2)}{\delta t}d\mathbf{k}_2 = -\frac{\delta n(\mathbf{k}_3)}{\delta t}d\mathbf{k}_3 = -\frac{\delta n(\mathbf{k}_4)}{\delta t}d\mathbf{k}_4 \quad (6)$$

where  $\delta n(\mathbf{k})/\delta t$  indicates the action transfer that is due to this particular resonance combination. As shown in Equation (3.6),  $\delta n(\mathbf{k}_i)d\mathbf{k}_i/\delta t$  ( $i=1, 2, 3, 4$ ) are the equal magnitude but are different in sign. Accordingly, if we calculate  $\delta n(\mathbf{k})/\delta t$  for one component of the resonant four waves, then we immediately know  $\delta n(\mathbf{k})/\delta t$  for the other three components. The other type of symmetry is associated with the geometrical similarity of resonance configurations. One is the mirror image of a resonance combination that has the same interaction coefficient as the original one. The other is a rotation of a resonance combination that also gives the same interaction coefficient.

Now, we specify a particular wave number vector  $\mathbf{k}_4$  (with  $\omega_4$  and  $\theta_4$ ) at which the non-linear energy transfer is to be evaluated, and then assume the sequence of frequencies as follows, considering the first kind of symmetry of the non-linear wave-wave interaction so as to eliminate the overlap computations.

$$\omega_3 \leq \omega_1 \leq \omega_2 \leq \omega_4 \quad (7)$$

For the computation of realistic continuous energy transfer of  $\partial n(\omega, \theta)/\partial t$ , the computation must be carried out with the loops of frequency  $\omega_4$  and direction and  $\theta_4$ . The computation of the configuration of resonant interactions are to be performed in advance with the computation of variables such as  $\tilde{G}$ ,  $S$ , etc. in the Boltzmann integral for both regular and singular points. The details of the computation procedure are explained in Masuda (1980) and Komatsu and Masuda (1996).

#### The SRIAM method (approximate method)

The RIAM method turned out to have the same degree of accuracy as Masuda's rigorous method. Although the RIAM method is 300 times faster than Masuda's method, it is still a few thousand times slower than the DIA, simply because the RIAM method processes thousands of resonance configurations.

Hence, Komatsu (1996) developed a new scheme of practical efficiency with a slightly lower level of accuracy than the RIAM method. The method is called the Simplified RIAM (SRIAM) method, which processes 20 representative configurations chosen by some optimisation. The SRIAM method can be expressed by the following equation.

$$T(\omega_4, \theta_4) = \frac{\partial \phi_4}{\partial t} = (2\omega_4^{23}) \sum_{i=1}^{20} C_i \tilde{K}_i(\tilde{\theta}_1, \tilde{\Omega}, \tilde{\theta}_3) \{n_1 n_2 (n_3 + n_4) - n_3 n_4 (n_1 + n_2)\} \quad (8)$$

where  $\tilde{K}_i(\tilde{\theta}_1, \tilde{\Omega}, \tilde{\theta}_3) = 8\tilde{\omega}_1^3 \omega_3^4 \tilde{G} S^{-1} \Delta \tilde{\theta}_3 \Delta \tilde{\Omega} \Delta \tilde{\theta}_1$ , and  $C_i$ , ( $i=1, \dots, 20$ ) are the coefficients.

Komatsu (1996) listed the optimum 20 combinations of the resonant configurations as well as the optimum positive coefficients  $C_i$  tuned by some optimisation, where 7 configurations are chosen for singular points and the other 13 configurations are chosen for regular points from  $(\tilde{\theta}_1, \tilde{\Omega}, \tilde{\theta}_3)$  space.

It is noted that in the method of Komatsu (1996) the optimum resonant configurations and the coefficients  $C_i$  depend on how many configurations we choose as well as how many directional and frequency bins constitute the directional spectrum in the model. That is, the optimum resonant configurations and the coefficients  $C_i$  have to be re-determined for each different computation conditions. For these reasons, a simpler method is preferable to determine the optimum configurations and the coefficients  $C_i$ .

#### DIA method

The Discrete Interaction Approximation (DIA) was developed by Hasselmann et al. (1985). The full solution to the Boltzmann integral (Eq. 3) uses a very large set of wave quadruplets with many

different configurations, whereas the DIA uses a small number of quadruplets which all have the same configuration. The resonant conditions expressed by the following equations:

$$\left. \begin{array}{l} \omega_1 = \omega_2 = \omega \\ \omega_3 = \omega(1 + \lambda) = \omega_+ \\ \omega_4 = \omega(1 - \lambda) = \omega_- \\ \theta_1 = \theta_2 = \theta \end{array} \right\} \quad \left. \begin{array}{l} \theta_3 - \theta = \pm \cos^{-1} \left\{ \frac{1 + 2\lambda + 2\lambda^3}{(1 + \lambda)^2} \right\} \\ \theta_4 - \theta = \mp \cos^{-1} \left\{ \frac{1 - 2\lambda - 2\lambda^3}{(1 + \lambda)^2} \right\} \end{array} \right\} \quad (9)$$

where  $\lambda$  is a constant for determining the combination of the component waves. Hasselmann et al (1985) set  $\lambda = 0.25$  based on numerical experiments. The rates of change of the energy densities ( $\delta_{nl}$ ,  $\delta_{nl}^+$ ,  $\delta_{nl}^-$ ) with focused only on the configuration and simplified the Boltzmann integral are given by:

$$\left\{ \begin{array}{l} \delta \mathcal{S}_{nl} \\ \delta \mathcal{S}_{nl}^+ \\ \delta \mathcal{S}_{nl}^- \end{array} \right\} = \left\{ \begin{array}{l} -2(\Delta\omega\Delta\theta)/(\Delta\omega\Delta\theta) \\ (1 + \lambda)(\Delta\omega\Delta\theta)/(\Delta\omega_+\Delta\theta) \\ (1 - \lambda)(\Delta\omega\Delta\theta)/(\Delta\omega_-\Delta\theta) \end{array} \right\} \times C\omega^{11}g^{-4} \left[ F^2 \left\{ \frac{F_+}{(1 + \lambda)^4} + \frac{F_-}{(1 - \lambda)^4} \right\} - 2 \frac{FF_+F_-}{(1 - \lambda^2)^4} \right] \quad (10)$$

where  $F \equiv F(\omega, \theta)$ ,  $F_+ \equiv F(\omega_+, \theta)$ ,  $F_- \equiv F(\omega_-, \theta)$  are the energy densities at the values of the interacting wave numbers,  $g$  is the gravitational acceleration,  $C$  is a constant equal to  $3 \times 10^7$ . In addition, DIA gives poor accuracy in the case of sharp-shaped spectra such as the JONSWAP spectrum although it gives good performance for wide-shaped spectra such as the Person-Moskowitz spectrum (Hashimoto and Kawaguchi, 2001). The advantage of DIA is, however, not its accuracy, but is in its retention of many important physical characteristics of nonlinear interactions, and its robustness when applied in a practical wave model (Tolman, 2003).

#### FD-RIAM method (Hashimoto et al, 2002)

RIAM, SRIAM, and DIA method only apply to deep-water waves. Hashimoto et al. (1998) proposed a computational method for calculating the non-linear energy transfer in finite-depth gravity wave spectra, by extending the exact methods for deep water of Masuda (1980) and Komatsu and Masuda (1996; i.e., the RIAM method). It involves reducing the Boltzmann integral for finite-water depth as follows,

$$\frac{\partial \phi(\omega_4, \theta_4)}{\partial t} = \frac{2\omega_4 k_4}{C_g(k_4)} [d\tilde{\theta}_3] d\Omega [d\tilde{\theta}_1] \left\{ \frac{k_1 k_3 \omega_3}{C_g(k_1) C_g(k_3)} \frac{G}{S} \right\} \{n_1 n_2 (n_3 + n_4) - n_3 n_4 (n_1 + n_2)\} \quad (11)$$

where  $\tilde{\theta}_1 = \theta_1 - \theta_a$ ,  $\tilde{\theta}_2 = \theta_2 - \theta_a$ ,  $\tilde{\theta}_3 = \theta_3 - \theta_4$ ,  $\Omega = \ln \omega_3$  and the denominator  $S$ , arising from  $\delta(\omega_1 + \omega_2 - \omega_3 - \omega_4)$ , is given by

$$S = \left| 1 + \frac{C_g(k_2)}{C_g(k_1)} \left\{ \frac{k_1 - k_a \cos(\theta_1 - \theta_a)}{k_2} \right\} \right| \quad (12)$$

The detail explanation of the derivation of above equations and the computation method of FD-RIAM are described in Hashimoto et al., (1998, 2002).

#### Initial conditions of directional spectrum for computations of the nonlinear energy transfer

Characteristics of the nonlinear energy transfer is polymorphous depending on the energy distribution of directional spectrum. In order to investigate the characteristics of the nonlinear energy transfer, first we have to assume directional spectrum for the computation. In this study, we assumed the directional spectrum as  $s(f, \theta) = s(f)G(\theta|f)$ , where the frequency spectrum  $S(f)$  and the directional function  $G(\theta|f)$  are assumed as follows:

$$S(f) = \sum_i \alpha_i H_{1/3}^2 T_{pi} (f/f_{pi})^{-m_i} \exp\left\{ -(m_i/n_i)(f/f_{pi})^{-n_i} \right\} \gamma_i^{\exp\left\{ -(f/f_{pi}-1)^2/2\sigma^2 \right\}} \quad (13)$$

$$\text{Where, } f_p = \left[ 1 - 0.132(\gamma + 0.2)^{-0.559} \right] / T_{1/3}, \quad \sigma = \begin{cases} 0.07 & (0.7f_p < f < f_p) \\ 0.09 & (f_p \leq f < f_p) \end{cases}$$

$$G(\theta|f) = \sum_i \beta_i \cos^{2S_i} \left\{ \left( \theta - \bar{\theta}_i \right) / 2 \right\} \quad (14)$$

$$\text{Where, } S = \begin{cases} S_{\max} (f / f_p)^5 & (f < f_p) \\ S_{\max} (f / f_p)^{-2.5} & (f \geq f_p) \end{cases}$$

For the simulations of unimodal directional spectrum, the suffix  $i$  is with  $i = 1$  only, while two different wave groups with different sets of parameters,  $H_{1/3}$ ,  $T_{1/3}$ ,  $\gamma_i$ ,  $S_i$ ,  $\theta_i$ : ( $i = 2$ ), are superposed for bimodal directional spectrum.  $\alpha_i$  and  $\beta_i$  are proportionality coefficients.

When discussing possible frequency downshift for the cases under the wind wave conditions, it should be noted that a formula (Equation (15), Goda, 2003) obtained from the Wilson's formulas for wind waves should be taken into account.

$$T_{1/3} \cong 3.3(H_{1/3})^{0.63} \quad (15)$$

That is, the formula gives the maximum  $H_{1/3}$  under a given  $T_{1/3}$  (as shown in Fig. 1).

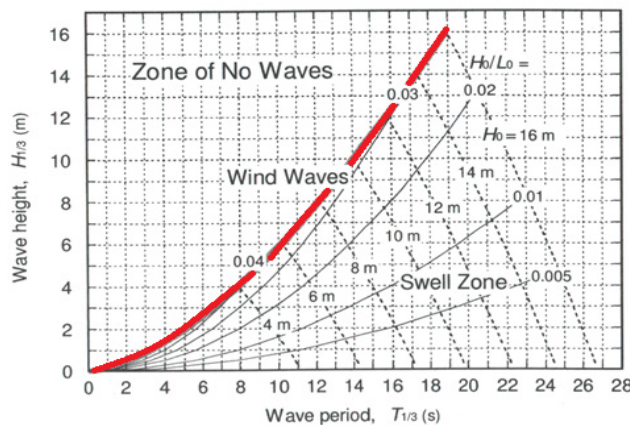


Figure 1. The steepness of wind waves (This figure is cited from Fig. 3.4 in Goda (2010).)

## RESULTS OF NUMERICAL SIMULATIONS

### Long-term evolution of frequency spectra computed by WAM with RIAM, SRIAM, and DIA

As an initial value, JONSWAP type spectrum and Mitsuyasu's directional function are assumed with  $\gamma = 3.3$ , peak frequency  $f_p = 0.1\text{Hz}$ , and directional concentration parameter  $S_{\max} = 15$ . Figure 2 shows examples of long-term evolution of frequency spectra computed by taking account of only the nonlinear energy transfer  $S_{nl}$ , without the wind input ( $S_{in} = 0$ ), and the dissipation ( $S_{dis} = 0$ ). They are computed in duration-limited conditions for 120 hours using the DIA, RIAM, and SRIAM. Thick line in Fig. 2 shows the initial spectrum, thin lines illustrate the evolutions of the spectra at 15, 30, 45 minutes, and 1, 2, 6, 12, 24, 48, 72, 96, 120 hours. The horizontal axis is the frequency  $f$ , and the vertical axis shows the normalized energy density divided by the peak value of the initial spectrum.

As seen in Fig. 2, the peak frequency initially located at 0.1Hz moves toward lower frequency side in all cases of RIAM, SRIAM, and DIA. The amount of the energy downshift seems to be large in early stage, then slowly decays over time. During the time, the energy distributions of frequency spectra incline toward the low frequency side gradually. RIAM and SRIAM show smooth and continuous frequency downshift in frequency spectra, while DIA shows relatively discontinuous frequency downshift. The evolution of the spectra by RIAM shows narrower shapes than those by SRIAM and DIA. The peak values of the spectra in RIAM tend to overshoot, and considerable differences are seen in those of DIA and SRIAM. Comparing with them in detail, the way of energy transfer seems to be different in each method, especially between DIA and the others. That is, the spectral peaks computed with DIA reduce once with downshift, and then increase again although the spectral peaks of RIAM and SRIAM show monotonous and continuous downshift.

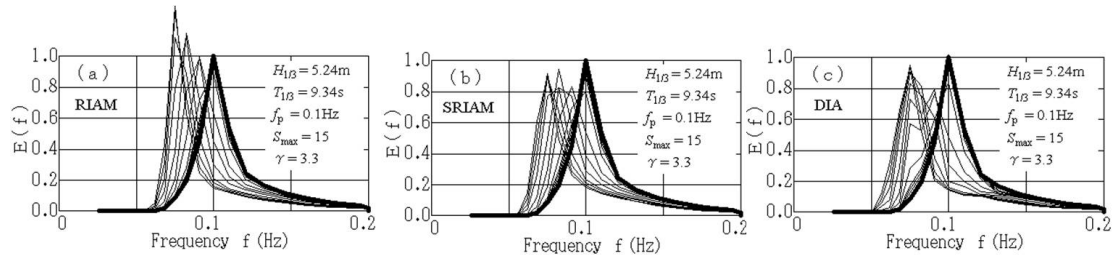


**Figure 2. Long-term evolution of frequency spectra by (a) RIAM, (b) SRIAM, and (c) DIA**

Figure 3 shows long-term evolution of frequency spectra computed by taking account of the nonlinear energy transfer  $S_{nl}$  and the energy dissipation  $S_{dis}$  under the same conditions as those in Fig. 2. Smooth and continuous downshift of the spectral peaks can be seen in those computed with RIAM and SRIAM. On the other hand, an unreasonable results are seen in the spectra computed with DIA, where the peaks become smaller once and then increase thereafter.

Since the frequency downshift computed with DIA shows rough in Fig. 3, we evaluated the behavior of the nonlinear energy transfer in each time step computed with RIAM, SRIAM, and DIA. Figure 4 shows the time evolution of one dimensional nonlinear energy transfer functions  $S_{nl}(f)$  as a function of frequency  $f$ , where  $S_{nl}(f, \theta)$  was integrated with respect to the direction  $\theta$ . Thick lines in the figures are the initial values of the nonlinear energy transfer corresponding to the each initial directional spectrum. The thin lines are the evolutions of nonlinear energy transfer corresponding to the spectra shown in Fig. 3, respectively. As seen in Fig. 4, the intensity of of the nonlinear energy transfer by RIAM and SRIAM show gradual decreases with the downshift of the spectral peak and the decrease of wave steepness, while the DIA shows two negative extreme values. As seen in Fig.4, although the distributions of the nonlinear energy transfer between RIAM and SRIAM are similar, they are very different from those of DIA. The locations and maginitudes of the negative extreme values of the nonlinear energy transfer of RIAM are slightly different those of SRIAM, but are very differnt from those of DIA.

Judging from these results, RIAM and SRIAM have similar characteristics inherently. In the following, therefore, we will discuss the characteristics of the frequency downshift on the basis of the numerical results computed with SRIAM, a practical computation method for deep water waves.

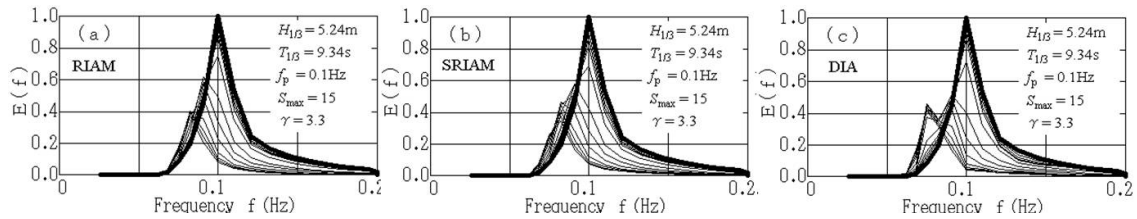


**Figure 3. Long-term evolution of frequency spectra by RIAM, SRIAM, and DIA ( $S_{nl}$  and  $S_{dis}$  are applied.)**

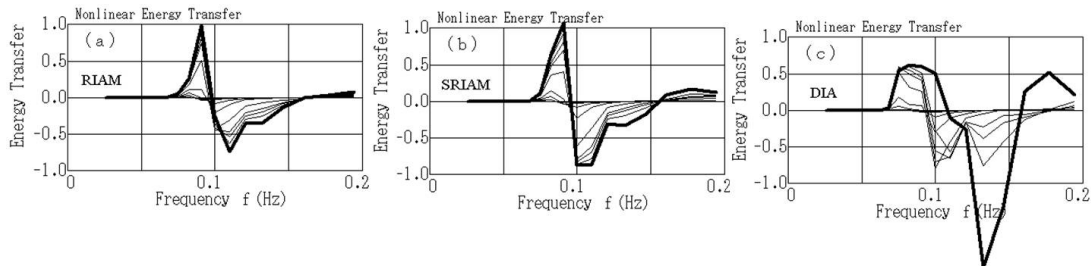


**Figure 4. Long-term variation of the nonlinear transfer  $S_{nl}$  by RIAM, SRIAM, DIA (correspond to Figure 3)**

**Relation between frequency downshift and wave steepness  $H/L$**

Figure 5 shows examples of the time evolutions of the frequency spectra, where JONSWAP spectra and Mitsuyasu’s directional functions are assumed as the initial conditions of directional spectra. In each panel in Fig. 5, the peak frequencies (the significant wave periods) are assumed to be the same ( $f_p = 0.1\text{Hz}$ ), while the significant wave heights are different in each case. In case (a) the maximum wave height are assumed with Goda’s formula Eq. (15) as the possible maximum significant wave height, i.e., the maximum wave steepness under the condition of  $f_p=0.1\text{ Hz}$ . That is, the magnitude of the wave steepness is (a), (b), and (c) in descending order. As seen in the Fig. 5, intensity of frequency downshifts due to the nonlinear energy transfer is reduced with the decrease of the wave steepness.

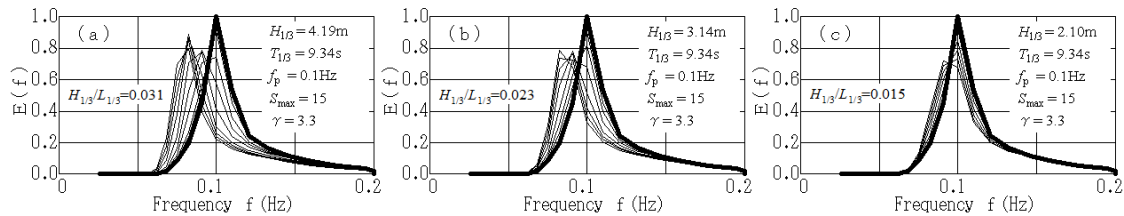


**Figure 5. Relation between frequency downshift and wave steepness  $H/L$  ( $f_p = \text{const.}$ ) in time evolution of frequency spectra ( $S_{nl}$  is computed by SRIAM)**

**Relation between frequency downshift and peak frequency  $f_p$**

Figure 6 shows examples of time evolutions of frequency spectra, where energy concentration parameters are assumed to be the same, i.e.,  $\gamma = 3.3$  and  $S_{\text{max}} = 15$  in all cases, while the peak frequencies are respectively assumed as  $f_p = 0.047\text{ Hz}$  in (a),  $0.075\text{ Hz}$  in (b), and  $0.133\text{ Hz}$  in (c). In each case, the significant wave periods are determined based on Eq. (13) as  $T_{1/3} = 20.03\text{s}$  in (a),  $12.44\text{s}$  in (b), and  $7.02\text{s}$  in (c), respectively. Then, the significant wave heights,  $H_{1/3}$  are determined by Eq. (15) as the possible maximum values as wind waves, i.e., the steepest waves in a statistical sense under each wave condition. As seen in Fig. 6, intensity of frequency downshift due to the nonlinear energy transfer is more intense in cases where the peak frequencies are at higher frequencies. That is, the intensity of frequency downshift seems to decrease with the decrease of  $f_p$  (with the increase of  $T_{1/3}$ ) even under the condition of the maximum  $H_{1/3}$ . This may indicate that there seems to be a maximum limit in the significant wave period. Our numerical experiments indicate that possible frequency downshift caused by the nonlinear energy transfer is up to  $T_{1/3} \approx 30\text{s}$  approximately at a maximum. Longer waves than  $T_{1/3} \approx 30\text{s}$  can not be generated by the nonlinear energy transfer under reasonable initial wind wave conditions in  $H_{1/3}$  and  $T_{1/3}$ .

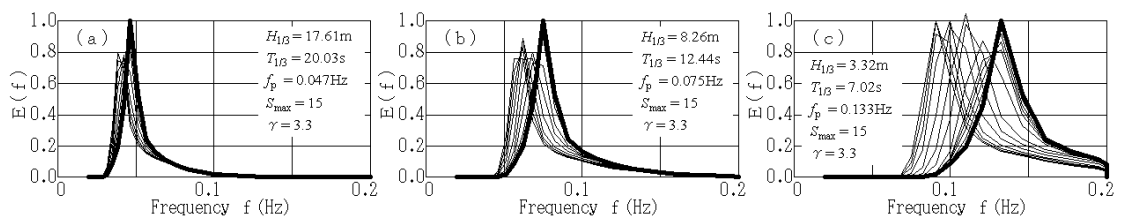


**Figure 6. Relation between frequency downshift and peak frequency  $f_p$  in time evolution of frequency spectra ( $S_{nl}$  is computed by SRIAM)**

**Relation between frequency downshift and energy concentration parameters**

Figure 7 (a), (b), and (c) show examples of evolutions of frequency spectra computed under the same condition with the peak frequency  $f_p = 0.075\text{Hz}$ , while the combination of energy concentration parameters  $\gamma$  and  $S_{\text{max}}$  are different with each other, i.e.,  $\gamma = 3.3$  and  $S_{\text{max}} = 75$  in (a),  $\gamma = 7.0$  and  $S_{\text{max}} = 15$  in (b),  $\gamma = 7.0$  and  $S_{\text{max}} = 75$  in (c). Depending of the differences in  $\gamma$  and  $S_{\text{max}}$ , the significant wave height  $H_{1/3}$  and the period  $T_{1/3}$  are slightly different due to Eqs.(13) and (15), i.e.,  $H_{1/3} = 8.26\text{m}$  and  $T_{1/3} = 12.44\text{s}$  in (a),  $H_{1/3} = 8.56\text{m}$  and  $T_{1/3} = 12.73\text{s}$  in (b),  $H_{1/3} = 8.56\text{m}$  and  $T_{1/3} = 12.73\text{s}$  in (c). In addition, Fig.6 (b) and Fig. 7 (a) are computed with almost the same conditions except  $S_{\text{max}}$ , i.e.,  $S_{\text{max}} = 15$  in Fig.6 (b), while  $S_{\text{max}} = 75$  in Fig.7 (a). Compared Fig.6 (b) with Fig. 7 (a), and Fig. 7 (b) with Fig.7 (c),

the intensity of frequency downshift seems to increase with the increase of the energy concentration parameters  $\gamma$  and  $S_{max}$ .

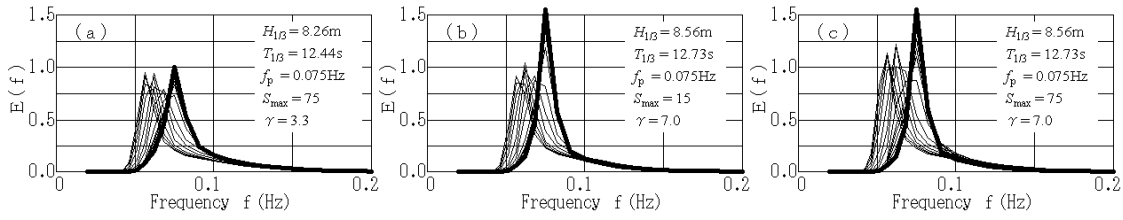


Figure 7. Relation between frequency downshift and energy concentrate parameters ( $S_{max}$  and  $\gamma$ )

### Characteristics of frequency downshift in bimodal spectra

We investigate characteristics of the nonlinear energy transfer in various bimodal spectra. Figure 8 shows the evolutions of bimodal spectra computed with SRIAM, where the spectra having the peak frequency at  $f_p = 0.1\text{Hz}$  are assumed with  $\gamma=3.3$  and  $S_{max}=15$  in each panel (a), (b), and (c), while spectra on lower frequency side are assumed with  $f_p = 0.08\text{Hz}$ ,  $\gamma = 7.0$  and  $S_{max} = 75$  in (a),  $f_p = 0.075\text{Hz}$ ,  $\gamma=7.0$  and  $S_{max}=75$  in (b), and  $f_p = 0.07\text{Hz}$ ,  $\gamma=7.0$  and  $S_{max}=75$  in (c), respectively. The crossing angle  $\Delta\theta$  between the principal wave propagation directions of two wave groups is assumed to be  $\Delta\theta=0^\circ$  in all cases of (a), (b), and (c). That is, the ratios between two peak frequencies in each case are 0.8 in (a), 0.75 in (b), and 0.7 in (c), respectively. The other parameters are assumed to be the same.

As seen in Fig. 8, by the influence of the nonlinear energy transfer  $S_{nl}$ , the energy distributions of the bimodal spectra gradually change into unimodal ones where the peaks on higher frequency gradually disappear. Although clear frequency downshift can be seen in (a), where ratio between two peak frequencies is relatively larger ( $f_{p1}/f_{p2} = 0.80$ ), while no frequency downshift can be observed in (c), where  $f_{p1}/f_{p2} = 0.70$ . Intensity of frequency downshift in (b) is between (a) and (c). That is, the intensity of frequency downshift decreases with the decrease of frequency ratio of  $f_{p1}/f_{p2}$ . Similar phenomena had been reported in previous studies (e.g., Masuda, 1980, Komatsu et.al, 1996).

Figure 9 shows examples of evolutions of frequency spectra computed under the same condition as those in Fig. 8 (a) except the crossing angle  $\Delta\theta$ . The cases (a), (b) and (c) in Fig. 9 are computed with  $\Delta\theta$  are  $30^\circ$ ,  $60^\circ$ , and  $90^\circ$ , respectively. Predominant frequency downshift can be seen in Fig. 8 (a) where  $\Delta\theta = 0^\circ$ . As seen in Fig. 8 (a) and Fig. 9, the intensity of frequency downshift decreases with the increase of  $\Delta\theta$ . Masson (1993) investigated the nonlinear energy transfer for a swell of finite bandwidth and indicated a maximum coupling when the swell direction is about  $40^\circ$  to the mean direction of the short waves. The results in Fig. 8 and 9 seem to be different from that of Masson.

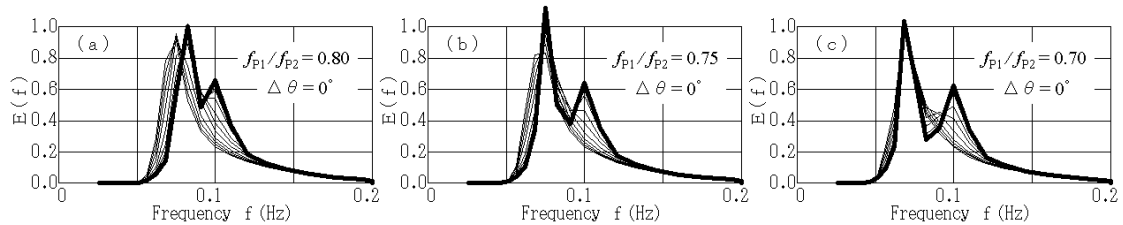


Figure 8. Characteristics of frequency downshift in bimodal spectra with different  $f_{p1}/f_{p2}$  ( $S_{nl}$  is computed by SRIAM)

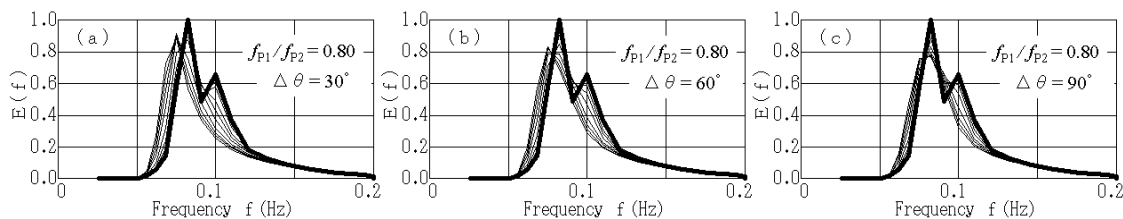


Figure 9. Characteristics of frequency downshift in bimodal spectra with different  $\Delta\theta$  ( $S_{nl}$  is computed by SRIAM)

**Investigation of frequency downshift of spectra in finite water depths by FD-RIAM**

We investigate the characteristics of the nonlinear energy transfer,  $S_{nl}(f, \theta)$ , of various directional spectra in deep and finite water depths with FD-RIAM since RIAM, SRIAM, and DIA can only be applied to deep water waves. As the initial conditions for the computations, the directional spectra are assumed with Eqs. (13) and (14). Figure 10 shows examples of one dimensional nonlinear energy transfer functions,  $S_{nl}(f)$ , as a function of frequency  $f$ , where  $S_{nl}(f, \theta)$  are integrated with respect to the direction  $\theta$ . The left and center panels, (a1), (a2), (b1), and (b2) are computed with  $\gamma = 1.0$  as the Pierson–Moskowitz (PM) type spectra, while the right panels, (c1) and (c2) are computed with  $\gamma=3.3$  as the JONSWAP type spectra. The differences between (a1) and (b2) or (a2) and (b2) are a parameter in directional function in Eq. (14). That is, the directional energy concentration parameter  $S$  is assumed to be constant as  $S = 2$  in (a1) and (a2), while directional function is assumed as a function of frequency  $f$  by assuming  $S_{max} = 10$  in (b1) and (b2).

The upper panels, (a1), (b1), and (c1) are examples of  $S_{nl}(f)$  computed under the conditions of  $k_p h = 8.0, 1.0,$  and  $0.8,$  respectively, while the lower panels, (a2), (b2), and (c2) are the ones computed under the conditions of  $k_p h = 0.8, 0.65,$  and  $0.6,$  respectively. It should be noted that the example of  $S_{nl}(f)$  computed with  $k_p h = 0.8$  is shown in both the upper and the lower panels for convenience. That is, as seen in Fig. 10, the absolute values of  $S_{nl}(f)$  increase with the decrease of  $k_p h$ , and the value under  $k_p h = 8.0$  is very different from that under  $k_p h = 0.6$ . Therefore, it seems inconvenient to show all the results in the same panel. Instead, these results are separated into the upper and the lower panels, and the value under  $k_p h = 8.0$  is shown in both panels as a reference value.

As seen in Fig. 10, although the distributions of  $S_{nl}(f)$  are very different in each case, there seems to be common features in that the intensity of the nonlinear energy transfer  $S_{nl}(f)$  increases with the decrease of the relative water depth  $k_p h$  and the positive peak of  $S_{nl}(f)$  moves toward lower frequency side as  $k_p h$  decreases.

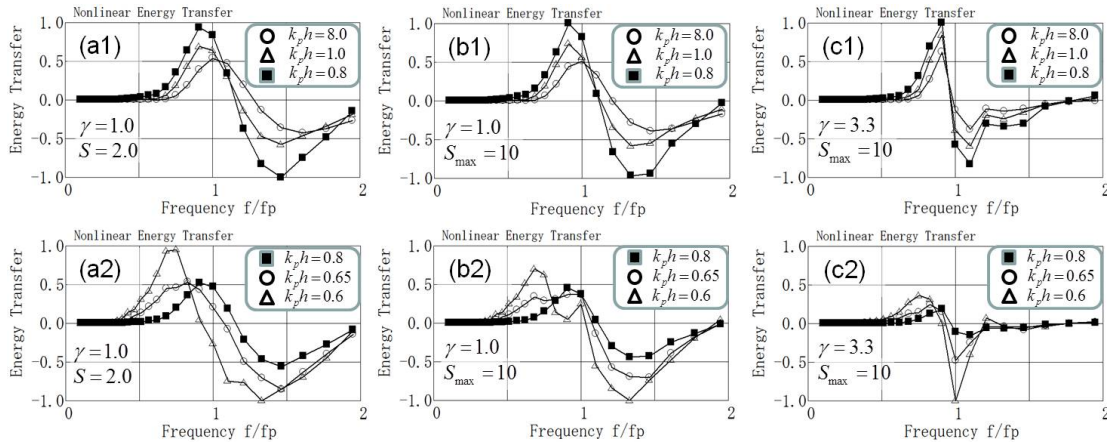


**Figure 10. One-dimensional nonlinear energy transfer functions for PM spectrum (a and b) and JONSWAP spectrum (c) in several water depths.**

**Enhancement factor and downshift factor**

Computations of the nonlinear energy transfer for directional spectra in finite water depths are more complicated and time consuming than those in deep water depths. In the third generation wave models, therefore, an enhancement factor  $R$  is introduced to convert the nonlinear energy transfer in deep water depth to that in finite water depth, and is expressed by:

$$S_{nl}(\text{finite depth}) = R(\bar{k}h)S_{nl}(\text{infinite depth}) \tag{15}$$

where  $\bar{k}$  is the mean wave number and  $S_{nl}(\text{infinite depth})$  is the nonlinear energy transfer computed by DIA for waves in deep water depth.

Enhancement factor  $R$  in DIA is expressed by the following equation:

$$R(x) = 1 + \frac{5.5}{x} \left(1 - \frac{5x}{6}\right) \exp\left(-\frac{5x}{4}\right), \quad \text{where } x = (3/4)\bar{k}h \quad (16)$$

Although the TMA spectrum (Bouws, 1985) seems to be a suitable one for expressing shallow water waves (Tsagareli, et al., 2005), however in the following, we will apply the same types of directional spectra used for deep water waves to investigate differences in characteristics of the nonlinear energy transfer and frequency downshift between deep water waves and finite water waves. In this sense, the following discussions may be merely comparative studies just for convenience. In the near future, we will show and discuss the results applied to TMA spectrum in other chances.

The plotted marks,  $\blacksquare$ ,  $\circ$ , and  $\triangle$ , in Fig. 11 indicate the enhancement factors  $R$  (in upper panels) and downshift factors (in lower panels) computed by FD-RIAM for various directional spectra in several water depths. The enhancement factor  $R$  in Fig. 11 is defined by the ratio of the maximum of nonlinear energy transfer for finite-depth waves to that for deep water waves computed by FD-RIAM. The downshift factor is defined by the ratio of the frequency of transfer maximum for finite-depth waves to that for deep water waves computed by FD-RIAM. As a reference, the enhancement factor ' $R$ ' (Eq. (16)) adopted in WAM is shown as a solid lines in the upper panels. The results shown in the left panels (a1) and (a2) in Fig. 11 are those computed for the directional spectra with the directional energy concentration parameter  $S$  being assumed as  $S=2$ . The results in the middle panels, (b1) and (b2), and the right panels, (c1) and (c2), are computed with  $S_{\max}=10$  and  $S_{\max}=25$ , respectively. That is, the directional distributions of directional spectra assumed in (b) are wider than those in (c). The marks,  $\blacksquare$ ,  $\circ$ , and  $\triangle$ , in each panel indicate the results computed under the conditions with  $\gamma=1.0$ , 3.3, and 7.0, respectively. As seen in the upper panels, the characteristics of the enhancement factor  $R$  are different depending on the energy distribution of directional spectra. That is,  $R$  shows better agreement with those computed by FD-RIAM in the cases of smaller  $S_{\max}$  and  $\gamma$ . Stated differently,  $R$  shows better agreement for broader directional spectra, but does not so for narrow directional spectra in frequency and direction. It should be noted that  $R$  is not a monotonous function in the cases of narrower directional spectra.

Since  $R$  works only for the enhancement of the energy distribution, and does not work for the frequency downshift, the downshift factor therefore seems to be more important than the enhancement factor. As seen in the lower panels in Fig. 11, although the frequency downshift factors of the broader spectra with  $\gamma=1.0$  gradually change to smaller values and return to around the original values as the relative water depth  $x$  decreases, while those of the narrow spectra with  $\gamma=3.3$  and 7.0 change to smaller values sharply as the relative water depth  $x$  decreases. In other words, although the behaviour of frequency downshift factors of the broader spectra shows similar characteristics with those of the narrower spectra, the changes of the frequency downshift factor of the broader spectra to smaller values start at deeper water depths than those of the narrower spectra. In very shallow water depths, the downshift factors of the broader spectra suddenly change to very small values. This sudden changes might be due to an applicable limit of the nonlinear energy transfer of Eq. (3).

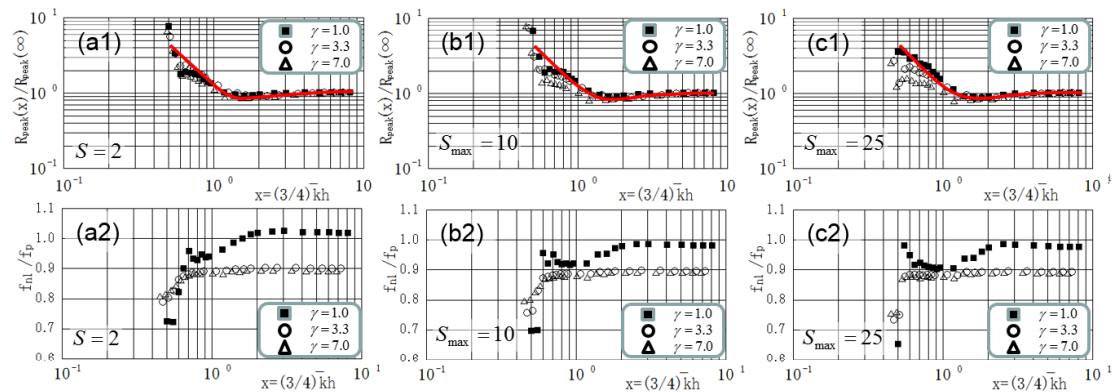
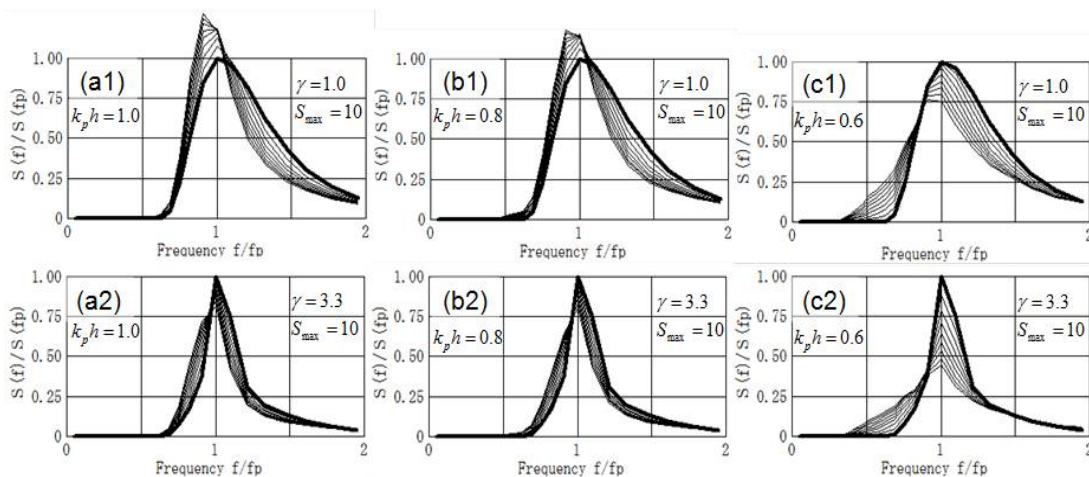


Figure 11. Enhancement factor (upper) and downshift factor (lower) for various directional spectra in several water depths. ( $x=(3/4)kh$ : nondimensional depth.)

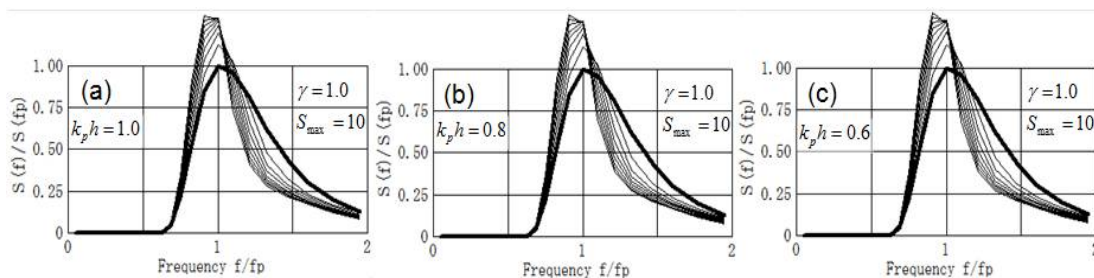
**Characteristics of duration-limited evolutions and frequency downshift of the spectra computed by FD-RIAM in finite water depths.**

Figure 12 shows duration-limited evolutions (for 2 hours) of frequency spectra computed by WAM with FD-RIAM, where only the nonlinear energy transfer term,  $S_{nl}(k_p h)$ , is taken into account in the source term. The evolutions of the spectra in finite water depths are much faster than those in deep water depths. There is little difference between (a) and (b), but is big difference between (c) and the others. Although the spectra evolve with changing its peak frequency toward the lower frequency side in the cases of deep water waves as seen in Fig. 2, the spectra in Fig. 12 (c) evolve by transferring the energy toward the lower frequency side with keeping the peak frequency at almost the same frequency and decreasing its magnitude.

In addition, we applied the original WAM with DIA to the same conditions of the upper panels in Fig. 12. The examples of the results are shown in Fig. 13. Strangely, the evolution of the spectra are almost the same regardless of the difference in water depths. This may be due to a ‘limiter’ introduced in WAM for suppressing divergence of the computations.



**Figure 12. Duration-limited evolutions (for 2 hours) of frequency spectra by FD-RIAM for PM (a1~c1) & JONSWAP spectra (a2~c2) in several water depths (only  $S_{nl}$  is applied.)**



**Figure 13. Duration-limited evolutions (for 2 hours) of frequency spectra by DIA with enhancement factor  $R$  for PM spectra in several water depths.**

**CONCLUSIONS**

This study evaluated the characteristics of the nonlinear energy transfer and the frequency downshift of the directional spectra with a third generation wave model, WAM, implemented with DIA (Hasselmann et al., 1985), RIAM (Komatsu et al., 1993) and SRIAM (Komatsu et al., 1996) in deep water waves. Numerical simulations on duration-limited evolutions of directional spectra were carried out with various initial conditions of directional spectra having various energy distributions in frequency and direction. As a result, interesting features are clarified, especially on the relation between frequency downshift and the energy concentration parameters of directional spectra. That is, intensity of frequency downshifts due to the nonlinear energy transfer is increased with the increase of energy concentration in frequency and direction. The characteristics of the frequency downshift of bimodal directional spectra are also discussed.

Characteristics of duration-limited evolutions and frequency downshift of the spectra in finite water depths were investigated with a modified WAM implemented with FD-RIAM (Hashimoto, et al., 1998, 2002). The evolution of directional spectra in finite water depths due to the nonlinear energy transfer was confirmed to be much faster than those in deep water depth. The enhancement factor  $R$  used in the third generation wave models as well as the downshift factor were also evaluated for various directional spectra in various water depths. Intriguingly, although the spectra evolve with changing its peak frequency toward the lower frequency side in deep water depth, the spectra in finite water depth,  $k_p h = 0.6$ , evolve by transferring the energy toward the low frequency, yet with keeping the peak frequency at almost the same frequency and decreasing its magnitude. Further investigation seems to be necessary.

## REFERENCES

- Banner, M. L. and Young, I. R., 1994, Modelling Spectral Dissipation in the Evolution of Wind Waves – Part 1. Assessment of existing model performances, *J. Phys. Oceanogr.*, 24, 1550-1671.
- Bouws, E., Gunther, H., Rosenthal, W. and C. L. Vincent, 1985, Similarity of the wind wave spectrum in finite-depth water, 1. Spectral form, *J. Geophys. Res.*, Vol. 90, 975-986.
- Goda, Y., 2003, Revisiting Wilson's Formulas for Simplified Wind-Wave Prediction, *J. Waterway, Port, Coastal, Ocean Eng.*, 129(2), 93-95.
- Goda, Y., 2010, Random seas and design of maritime structures 3<sup>rd</sup> edition, world scientific, 708p.
- Hashimoto N., H. Tsuruya and Y. Nakagawa, 1998, Numerical computations of the nonlinear energy transfer of gravity-wave spectra in finite water depths, *Coastal Engineering Journal*, 40, World Scientific, 23-40.
- Hashimoto, N and K. Kawaguchi, 2001, Extension and Modification of Discrete Interaction Approximation (DIA) for Computing Nonlinear Energy Transfer of Gravity Wave Spectra, *Proc. 4th Int. Symp. Waves 2001*, 530-539.
- Hashimoto, N., I. G. Haagsma and L. H. Holthuijsen, 2002: Four-wave interactions in swan. In *Proc. 28<sup>th</sup> Int. Conf. Coastal Eng., Cardiff, Wales*. ASCE, In Press.
- Hasselmann, K., 1962, On the non-linear energy transfer in a gravity-wave spectrum, Part 1, General theory, *Journal of Fluid Mechanics*, 12, 481-500.
- Hasselmann, K., 1963, On the non-linear energy transfer in a gravity-wave spectrum, Part 3, Evaluation of energy flux and sea-swell interactions for a Neuman spectrum, *Journal of Fluid Mechanics*, 15, 385-398.
- Hasselmann, K. et al., 1973, Measurements of wind waves growth and swell decay during the Joint North Sea Wave Project (JONSWAP), *Dt. Hydrogr. Z.*, A8(12), 95p.
- Hasselmann, S. and K. Hasselmann, 1981, A symmetrical method of computing the nonlinear transfer in a gravity wave spectrum, *Hamb. Geophys. Einzelschriften, Reihe A: Wiss. Abhand.*, 52, 138p.
- Hasselmann, S. and K. Hasselmann, 1985, Computations and Parameterizations of the Nonlinear Energy Transfer in a Gravity-Wave Spectrum. Part I: A New Method for Efficient Computations of the Exact Nonlinear Transfer Integral, *Journal of Physical Oceanography*, 15, 1378-1391.
- Komatsu, K., T. Kusaba and A. Masuda, 1993, An efficient method for computing nonlinear energy transfer among wind waves, *Bull. Res. Inst. Appl. Mech. Kyushu Univ.*, 75, 121-146 (in Japanese).
- Komatsu, K. and A. Masuda, 1996, A new scheme of nonlinear energy transfer among wind waves: RIAM method – algorithm and performance -, *Journal of Oceanography*, 52, 509-537.
- Komatsu, K. 1996, Development of a new generation wave forecasting model based on a new scheme of nonlinear energy transfer among wind waves, *Dr. Thesis, University of Kyushu*, 155p. (in Japanese).
- Komatsu, et al., 2001, Nonlinear energy transfer among wind waves in coastal region, *Bull. Fish. Res. Agen*, pp. 1, 7-21 (in Japanese).
- Masuda, A, 1980, Nonlinear energy transfer between wind waves, *Journal of Physical Oceanography*, 10, 2082-2092.
- Masson, D., 1993, On the nonlinear coupling between swell and wind waves, *J. Phys. Oceanogr.*, 23, pp.1249-1258.
- Resio, D. and W. Perrie, 1991, A numerical study of nonlinear energy fluxes due to wave-wave interactions, *Journal of Fluid Mechanics*, 223, 603-629.
- Roland, A., 2009, Development of WWM II — Spectral wave modelling on unstructured meshes, PhD Thesis, Darmstadt University of Technology, Institute for Hydraulic Engineering and Water Resources Management, Darmstadt, Germany.

- Tolman, H.L., 2003, Optimum Discrete Interaction Approximations for wind waves. Part 1: Mapping using inverse modeling. Tech. Note 227, NOAA/NWS/NCEP/MMAB.
- Tracy, B. A. and D. T. Resio, 1982, Theory and calculation of the nonlinear energy transfer between sea waves in deep water, *U. S. Army Engineer Waterways Experimental Station, Rep. No. 11*, Vicksburg, U. S. A.
- Tsagareli, K. N., A. V. Babanin, D. J. Walker, I. R. Young, 2005, A numerical Study of the Four-Wave Nonlinear Interactions in Finite-Depth Water, 17th Australasian Coastal and Ocean Engineering Conf and 10th Australasian Port and Harbour Conf, 299-304
- Ueno, K. and M. Ishizaka, 1997, On an efficient calculation method of the nonlinear energy transfer in wind waves, *Sottukojiho*, JMA, 64, 75-80 (in Japanese).
- Webb, D. J., 1978, Non-linear transfers between sea waves, *Deep-Sea Res.*, 25, 279-298.
- Young, I.R. ,1999, *Wind generated ocean waves*. Elsevier, Oxford, UK.